Desalination and Water Treatment
www.deswater.com
doi: 10.1080/19443994.2013.777368

51 (2013) 7586–7595
December

Taylor & Francis
Taylor & Francis Group

Fast and highly efficient removal of methylene blue by a novel EDTAD-modified magnetic chitosan material

Yunxue Xia[a,1], Xianxiang Dai[a,1], Shengtian Huang[b,1], Xiumei Tian[a], Hongyu Yang[a], Yunchun Li[a], Yu Liu[a], Maojun Zhao[a,*]

[a]*Department of Chemistry, College of Life and Science, Sichuan Agricultural University, Yaan 625014, P.R. China*
Tel. +86 835 8563240; Fax: +86 835 2862227; email: smlxy.sicau.edu.cn
[b]*School of Chemistry and Pharmaceutical Engineering, Sichuan University of Science and Engineering, Zigong 643000, P.R. China*

Received 14 January 2013; Accepted 10 February 2013

ABSTRACT

A novel adsorbent, ethylenediaminetetraacetic dianhydride (EDTAD)-modified magnetic chitosan (EMC) complex, was fabricated using glutaraldehyde as a cross-link agent. The obtained EMC was characterized by SEM, XRD, potentiometric titration, and FTIR. The results showed that nano-Fe_3O_4 with granular morphology were steadily integrated with chitosan and EDTAD was successfully modified on the surface of chitosan. The adsorption properties of EMC for methylene blue (MB) were then evaluated. Factors affecting the uptake behavior such as pH, contact time, initial concentration of MB, and temperature were investigated. The optimal adsorption conditions were determined as pH 6.0, MB concentration 300 mg L^{-1}, contact time 30 min, and temperature 35°C. The adsorption capacity in the optimal condition was 113.257 mg g^{-1}. The adsorption process followed the Sips isotherm model and the pseudo-second-order kinetic model. Desorption and regeneration experiments were conducted and the adsorption/desorption cycles of MB were repeated three times. The EMC regeneration efficiency and the MB recovery efficiency were 82.82% and 80.72%, respectively, in the third cycle by using HCl as the eluent solution.

Keywords: Chitosan; Magnetic; EDTAD; Methylene blue; Adsorption

1. Introduction

The presence and discharge of dyes in the environment is a matter of concern for both toxicological and esthetical reasons [1]. Industries such as textile, paper, plastics, etc., use dyes to color their products and produce abundant wastewater [2]. As a result, considerable colored wastewater without treatment is directly discharged into the river, which is adverse to the environment and human health. Methylene blue (MB) is the most commonly used dye for dying cotton, silk, and wood. On inhalation, it may cause difficult breathing, nausea, vomiting, profuse sweating, mental confusion, and methemoglobinemia [3,4]. Therefore, the treatment of dye wastewater is of great importance. At present, several physical, chemical, and biological decolorization methods have been reported.

*Corresponding author.

[1]*Yunxue Xia, Xianxiang Dai, Shengtian Huang contributed equally to this work.*

Amongst the numerous techniques of dye removal, adsorption is the superior choice and gives better results when used to remove various types of dyes [5,6].

Recently, natural polymer materials, mainly polysaccharides, have shown excellent potential in the field of water treatment, due to their low cost, availability, and advantageous presence of hydroxyl, amino, and other active functional groups. Among them, chitosan is a promising adsorbent for heavy metals and dyes [7]. Several chemical regents, such as maleic anhydride, polydimethylsiloxane, glycine, thiourea, and ethylenediamine, have been demonstrated to facilitate to enhance the adsorption capacity of chitosan when used to functionalize the polymer [8–12]. Studies on magnetic chitosan derivatives have mainly focused on the adsorption of mental ions [13–15]. However, few researches have reported the removal of dyes [16].

In this work, we developed an ethylenediaminetetraacetic dianhydride (EDTAD)-modified magnetic chitosan (EMC) composite by chelating environmental and cheap chitosan with nano-Fe_3O_4 and EDTAD. The adsorption behavior of EMC was examined by the Langmuir, Freundlich, Sips, and Temkin isotherm equations as well as the pseudo-first-order and the pseudo-second-order kinetic models. Batch studies were carried out to identify the optimum adsorption conditions such as pH, equilibrium time, initial MB concentration, and temperature. The EMC characteristics and adsorption mechanism were further examined by SEM, XRD, FTIR, and potentiometric titration analysis. Desorption and regeneration experiments were investigated as well.

2. Experimental methods

2.1. Chemicals

Chitosan with above 90% deacetylation degree and molecular weight of 1.5×10^5 was supplied by Shanghai blue season technology development Co., Ltd. The MB purchased from Tianjin Chemical Reagent No. 1 Plant, China, was selected as a representative reactive dye for this study. A stock solution of MB was prepared by dissolving 1.0 g of MB in 1 L of ultrapure water, the working solutions were obtained by dilution of the stock solution. Solution pH was adjusted by adding 0.1 M HCl and NaOH solution. All of the chemical reagents used were analytical grade. Ultrapure water with a esistivity of 18.23 MΩ cm^{-1} obtained from a pure water system (Ai Kuo, KL-UP-II-20, China) was used throughout the experiment.

2.2. Synthesis of EDTAD-modified magnetic chitosan (EMC)

2.2.1. Preparation of magnetic fluid (nano-Fe_3O_4)

The synthetic strategy of nano-Fe_3O_4 was based on the Shan zhi's method [17]. 2.592 g $FeCl_3{\cdot}6H_2O$ and 1.034 g $FeCl_2{\cdot}4H_2O$ were completely dissolved into 60 mL ultra pure water. Then, 20 mL ammonia was added into the mixture. After stirring at 80°C for 30 min, the reaction system was cooled to room temperature. Finally, the nano-Fe_3O_4 magnetic fluid was successfully prepared.

2.2.2. Preparation of magnetic chitosan (MC)

2.0 g of chitosan power was dissolved in 150 mL 0.2% acetic acid, the suspension was stirred at room temperature for 2–3 h, subsequently. The same volume of glutaraldehyde solution (1.5 wt.% in water) and 2.0 g nano-Fe_3O_4 after ultrasonication were successively added into the suspension. Then, the mixture was shaken at 200 rpm in a rotary shaker (DH2-DA, China), at 63°C for 2 h. The pH of reaction solution was maintained at pH 9–10 by adding sodium hydroxide solution. The resulting magnetic chitosan (MC) was collected by an external magnet and was washed thrice before it was freeze-dried in high vacuum for 24 h. Finally, MB was preserved in a desiccator for further use.

2.2.3. Preparation of EDTAD-modified magnetic chitosan (EMC)

2.0 g of EDTA dianhydride (EDTAD), synthesized following the method [18] described before, was added to 100 mL N, N-dimethylacetamide (DMAc) containing 2.0 g of MC in a three-neck round bottom flask equipped with a condenser. The mixture was stirred at 60°C for 4 h. Finally, the EMC was separated from the mixture by an external magnet and washed with adequate DMAc, ultra pure water, and 10% $NaHCO_3$ solution, respectively. The obtained EMC was freeze-dried in high vacuum for 24 h and preserved in a desiccator for further use.

2.3. Adsorption studies

The adsorption experiments were conducted in 250 mL conical flasks agitated at 150 rpm in a rotary shaker. For this, 0.1 g of EMC was mixed with 100 mL of MB solution at different initial concentration. The flasks were shaken for different time intervals at various temperatures and pHs. 0.1 mol L^{-1} HCl or 0.1 mol L^{-1} NaOH was added to adjust the initial pHs

of the solutions (3.0–8.0). After that, the supernatant was magnetically separated by an external magnetic field. The concentration of MB in the supernatant solution before and after adsorption was determined by spectrophotometer (V-1100D spectrophotometer, China) at λ_{max} of 664 nm. Each of the experiment was repeated thrice and the average values were obtained. The percentage removal (η) and the amount of MB adsorbed per unit mass EMC were calculated according to the following equations [12]:

$$\eta\ \% = \frac{(C_0 - C)}{C_0} \times 100 \quad (1)$$

$$q_e = \frac{(C_0 - C_{eq})V}{M} \quad (2)$$

where q_e is the equilibrium adsorption capacity (mg g^{-1}); C_0 is the initial concentration of MB in the experimental solution (mg L^{-1}); C_{eq} is the final or equilibrium concentration of the MB after adsorption (mg L^{-1}); V is the volume of the aqueous solution (L); and M is the amount of adsorbent (g).

2.4. Desorption and regeneration studies

After adsorption, the EMC adsorbent particles were separated by adding a magnetic field. Afterwards, 50 mL of various eluents (0.05 M HAc, 0.05 M HCl and absolute ethanol) were separately added into the washed EMC which was harvested by MB, stirring at 150 rpm for 30 min. After each cycle of recovery, the adsorbent was washed by ultra pure water and reused in the succeeding cycle. The MB recovery efficiency and the EMC regeneration efficiency could be calculated as follows:

$$\text{Recovery efficiency} = \frac{\text{Amount of dye desorbed}}{\text{Amount of dye adsorbed}} \times 100\% \quad (3)$$

$$\text{Regeneration efficiency} = \frac{\text{Regeneration adsorption capacity}}{\text{Original adsorption capacity}} \times 100\% \quad (4)$$

2.5. Characterization

The surface structure and morphology of chitosan, MC, and EMC were characterized using a scanning electron microscope (JSM-7500F, Japan) at a 5KV acceleration voltage. Prior to SEM analysis, the samples were coated with a thin layer of gold. The X-ray diffraction (XRD) pattern of nano-Fe_3O_4 and EMC were obtained by a diffractometer (Holland Philip-X'Pert Pro) with Cu Kα radiation ($\lambda = 0.15406$ nm) in steps of 0.03° (2θ) min^{-1} from 15° to 75° (2θ). Infrared spectra of chitosan, EMC before and after absorbed MB were measured using a Fourier transform infrared spectrophotometer (Shimadzu FTIR-8400s, Japan) within the range of 400–4,000 cm^{-1} through the KBr pressed-disk method. The active sites present on the surface of MC and EMC were determined by potentiometric titration on autotitrator (ZD-2, China) with a combined glass electrode. ProtoFit Version 2.0 [19–22], a useful software tool for the calculation of pK_a values as well as surface site densities of biological material, was employed to fit the acid–base titration data of MC and EMC.

3. Results and discussion

3.1. Experimental procedure

Fig. 1 shows the synthesis route to prepare EMC and provides a suggested mechanism for MB removal. The procedure includes four main steps. First, MC was composed by combining chitosan and nano-Fe_3O_4 via glutaraldehyde as a cross-linking agent. Second, EDTAD molecules were integrated with the MC via formation of ester/amido bond between EDTAD and hydroxyl/amine on the surface of MC. Third, after being rinsed by $NaHCO_3$ solution, more functional groups (carboxyl and amino groups) on EMC were exposed and the surface activity and water-solubility would be improved. Finally, the resulting EMC was conducted as a recycling magnetic adsorbent for the removal of MB in the aqueous solution.

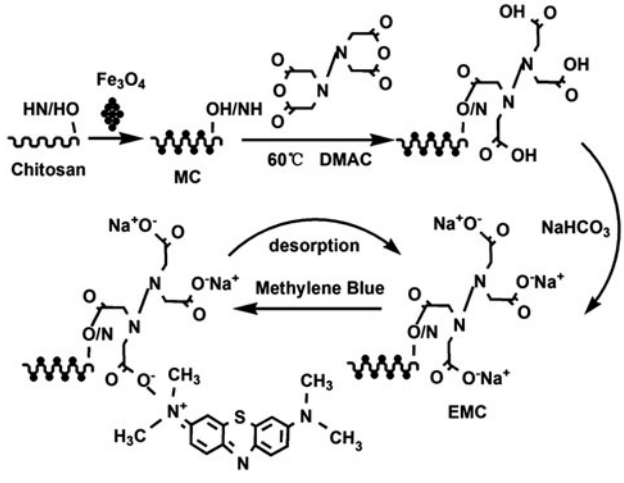

Fig. 1. Synthesis scheme of EMC and adsorption mechanism of MB on EMC.

3.2. Characterization

3.2.1. SEM analysis

Low- and high-magnification SEM images of pristine chitosan, MC, and EMC are shown in Fig. 2. It is important to note that irregular, porous, and creviced surface can be observed on pristine chitosan (Fig. 2 (A)). The SEM image of magnetic chitosan (Fig. 2(B)) shows more grain coalescence because of the integration between nano-Fe_3O_4 and chitosan. After EDTAD modification, the synthesized EMC surface (Fig. 2(C)) is relatively flat and nonporous because of the introduction of EDTAD.

3.2.2. XRD analysis

The XRD patterns of pure Fe_3O_4 and EMC are shown in Fig. 3, indicating the existence of iron oxide particles (Fe_3O_4). The XRD analysis results of pure Fe_3O_4 and EMC were mostly coincident. Six characteristic peaks for Fe_3O_4 ($2\theta = 30.20^\circ$, 35.48°, 43.08°, 57.11° and 62.60°), marked by their indices (2 2 0), (3 1 1), (4 0 0), (4 2 2), (5 1 1) and (4 4 0), were observed in two samples. These peaks reveal that the resultant magnetic particles were nano-Fe_3O_4 [23,24]. Compared with Fe_3O_4 particles, the characteristic peaks of EMC shifted slightly to lower angles. It could be attributed to the interaction occurring between chitosan and Fe_3O_4 particles. In addition, it can be seen that the XRD peak strength of EMC was lower than that of pure Fe_3O_4. This means the content of Fe_3O_4 for EMC was reduced in the experimental process.

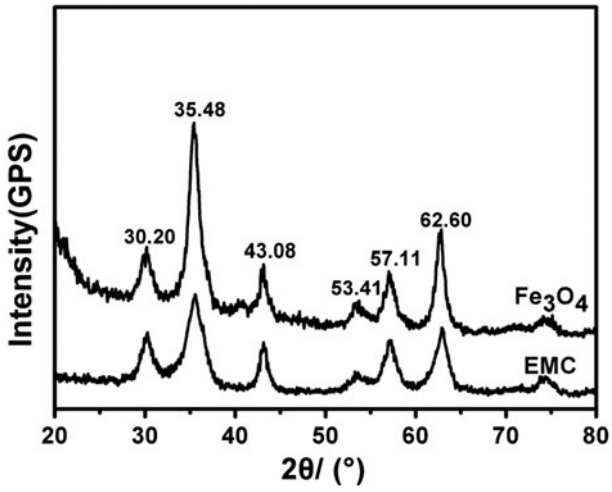

Fig. 3. X-ray diffraction spectra of nano-Fe_3O_4 and EMC.

3.2.3. Determination of active sites

In order to identify possible methylene blue binding sites, the functional groups on the surface of MC and EMC were determined by the potentiometric titration. Analysis of the titration data indicate that a three-site model in Protofit Version 2.0 software provided a good fit for MC and EMC. The acidity constants (pK_a) and site concentrations for each type of surface functional groups on MC and EMC are shown in Table 1. It is observed that the total concentrations of amine and hydroxyl groups on EMC are significantly higher than that on MC due to the introduction of EDTAD by esterification/amidation reaction. Meanwhile, the amount of carboxyl on EMC is much higher than that on MC. These phenomena indicate that although the esterification/amidation reaction occurred and consumed some hydroxyl/amino groups on the surface of EMC, more hydroxyl and amino groups on the surface of EMC were exposed resulting from the repeated vacuum freeze-drying in the preparation process of EMC. Thus, there were more functional groups on the surface of EMC, which might be helpful to the improvement of EMC adsorption capacity.

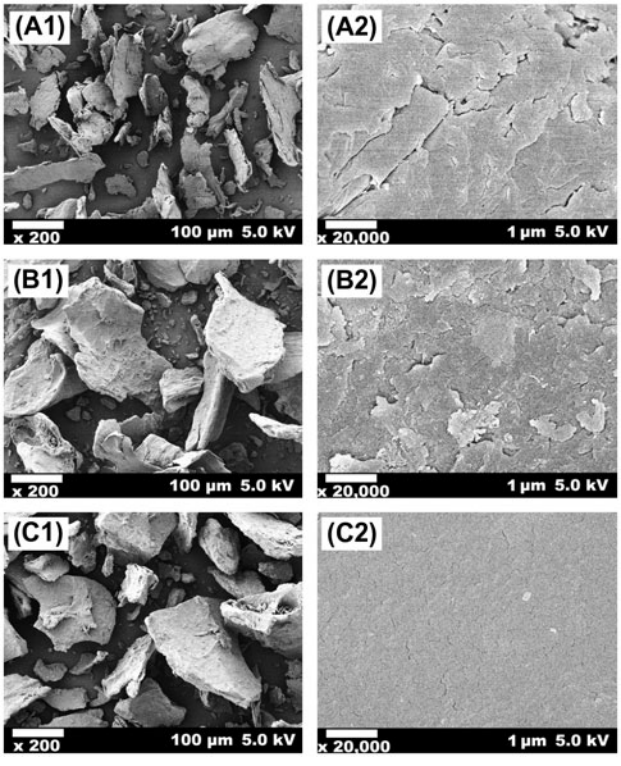

Fig. 2. SEM micrographs of nano-Fe_3O_4 (A1 and A2), MC (B1 and B2), and EMC (C1 and C2).

3.3. Effect of pH

Fig. 4 gives the adsorption capacity of EMC within pH range 3.0–8.0. The uptake of MB increased with

Table 1
Concentration and acidity constants for surface groups of MC and EMC MC/EMC: 3 g L^{-1}; titrant: 0.1 mol L^{-1} NaOH; reaction temperature: 25 ± 0.5°C; background electrolyte: 0.1 mol L^{-1} NaCl)

Adsorbent	Functional group	pK_a values reported	pK_a values obtained	Concentration of functional groups (m mol g^{-1})
MC	Carboxyl	2.00–6.00	5.00–5.55	0.65 ± 0.04
	Amine	9.00–11.00	9.69–10.20	0.25 ± 0.10
	Hydroxyl	8.00–12.00	10.90–11.90	0.09 ± 0.03
EMC	Carboxyl	2.00–6.00	4.56–4.70	0.88 ± 0.02
	Amine	9.00–11.00	9.00–9.50	0.50 ± 0.04
	Hydroxyl	8.00–12.00	9.35–10.45	0.49 ± 0.04

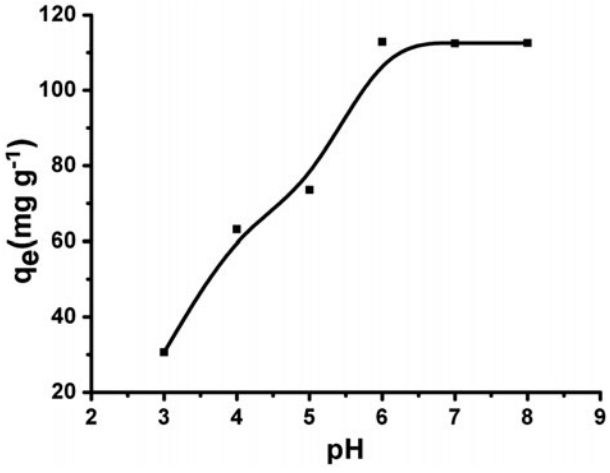

Fig. 4. Effect of the pH.

the increase of the solution pH with pH range from 3.0 to 6.0 and the maximum adsorption capacity of MB was 112.884 mg g^{-1} at pH 6.0. It can be noted that the adsorption phenomenon could occur even at low pH. It should be that at low pH values some protons were dissociated from carboxyl groups according to the acidity constant K_a of HEDTA [25]. Then, the positive-charged MB ions could bind with deprotonated carboxyl groups. However, at low pH values, the adsorption capacity was relatively low. This should be the competition of H^+ ions for binding sites on EMC. As the pH increased, most carboxyl groups and a small number of hydroxyl groups on the surface of EMC would be deprotonated. Thus, negative-charged functional groups could be integrated with positive-charged MB ions resulting in the increase of adsorption capacity at higher pH values. As is seen, the maximum adsorption capacity of MB occurred at pH6.0. When pH value was over 6.0, the adsorption capacity almost kept constant. This should be attributed to the limited functional groups especially carboxyl and hydroxyl groups. In the study, the optimum pH for MB adsorption was selected as 6.0.

3.4. Effect of contact time and kinetic studies

The effect of contact time on the adsorption of MB is shown in Fig. 5(a). The kinetic curve of MB indicates that the adsorption was rapid within the first

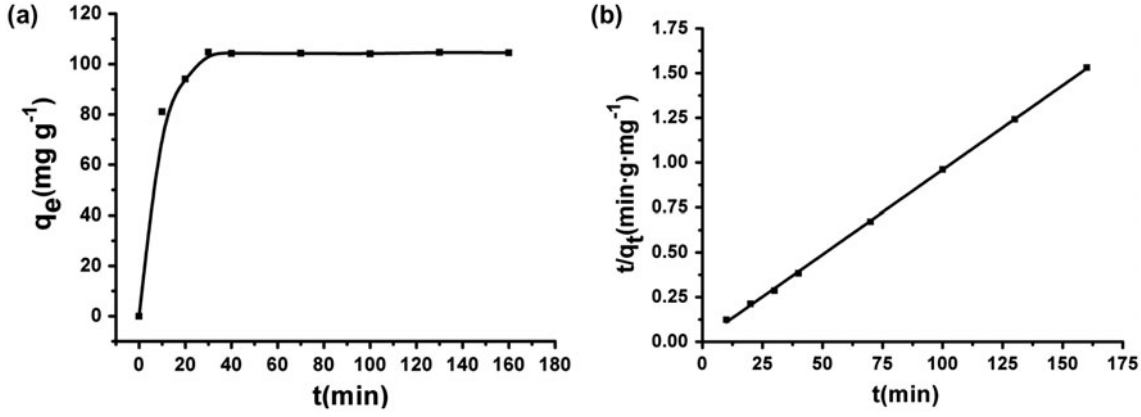

Fig. 5. Effect of the contact time (a) and pseudo-second-order kinetic isotherms of EMC (b).

10 min, and then slowed down apparently. It is observed that the amount of MB adsorbed (mg g^{-1}) increased with increasing contact time and reached equilibrium at about 30 min. Hence, 30 min was selected as the experimental contact time for further study.

In order to evaluate the kinetic mechanism that controls the adsorption process, pseudo-first-order and pseudo-second-order models were employed to interpret the experimental data [26]. A good correlation of the kinetic data would explain the adsorption mechanism of the dye on the solid phase [27]. The pseudo-first-order kinetic model and pseudo-second-order kinetic model were given in the following forms:

$$\ln(q_e - q_t) = -k_1 t + \ln q_e \quad (5)$$

$$\frac{t}{q_t} = \frac{1}{k_2 q_e^2} + \frac{t}{q_e} \quad (6)$$

where q_e and q_t (mg g^{-1}) refer to the adsorption capacity at equilibrium and time t, respectively, k_1 is the rate constant of pseudo-first-order equation (min^{-1}), k_1 can be calculated from the slopes of the linear plot of $\ln(q_e - q_t)$ vs. t. k_2 is the rate constant of pseudo-second-order equation (g mg^{-1} min^{-1}), k_2 can be calculated from the slopes of the linear plot of t/q_t vs. t.

The results of the kinetic parameters are shown in Table 2. The greater correlation coefficient ($R^2 = 0.99967$ of EMC) for pseudo-second-order kinetic model indicates that the adsorption of MB onto EMC fitted better to pseudo-second-order kinetic model. In addition, as is shown in Fig. 5(b), the theoretical value of q_e (105.932 mg g^{-1} for MB) obtained from pseudo-second-order model is closer to the experimental value (104.728 mg g^{-1} for MB), confirming the validity of that model to the adsorption system under consideration as well. This suggests the main adsorption mechanism of chemical adsorption. The adsorption of MB onto EMC may consist of two processes: the first process is interpreted to be the instantaneous adsorption stage or external surface adsorption. The second process is interpreted to be the gradual adsorption stage where intra particle diffusion controls the adsorption rate until finally the MB uptake reaches equilibrium.

3.5. Effect of initial MB concentration and adsorption isotherms

Fig. 6 gives the effect of initial MB concentration on adsorption. The results show that the adsorption capacity of MB on EMC increased till the MB uptake value reached the state of equilibrium. It is attributed to the collision efficiency between MB ions and EMC increasing with the increase in the initial concentration of MB in solution. However, meth adsorption capacity was no longer changed and remained almost constant after equilibrium. This was due to the lack of sufficient effective binding sites to accommodate the MB ions that were available in the solution [28].

In this study, the adsorption isotherms were investigated using four equilibrium models, which were Langmuir, Freundlich, Sips, and Temkin isotherm models. The Langmuir equation assumes that: (i) the solid surface presents a finite number of identical sites which are energetically uniform; (ii) there are no interactions between adsorbed species, meaning that the amount adsorbed has no influence on the rate of adsorption; and (iii) a monolayer is formed when the solid surface reaches saturation [29]. This model is expressed as:

$$q_e = \frac{b q_m C_e}{1 + b C_e} \quad (7)$$

Where C_e is the concentration of MB in solution at equilibrium (mg L^{-1}), q_e is the adsorption capacity at equilibrium (mg g^{-1}), q_m is the maximum adsorption capacity of the adsorbent (mg g^{-1}), and b is the Langmuir constant (L mg^{-1}) related to the affinity of binding sites.

Different from Langmuir isotherm model, the Freundlich isotherm expresses adsorption at multilayer and on energetically heterogeneous surface which can be expressed as Eq. (8).

Table 2
Comparison of the pseudo-first-order and pseudo-second-order adsorption rate constants and calculated and experimental q_e values

$q_{e\ exp}$ (mg g^{-1})	Pseudo-first-order kinetic model			Pseudo-second-order kinetic model		
	k_1 (min^{-1})	R^2	$q_{e\ cal}$ (mg g^{-1})	k_2 (g $mg^{-1}min^{-1}$)	R^2	$q_{e\ cal}$ (mg g^{-1})
104.728	0.03758	0.68803	19.931	0.005723	0.99967	105.932

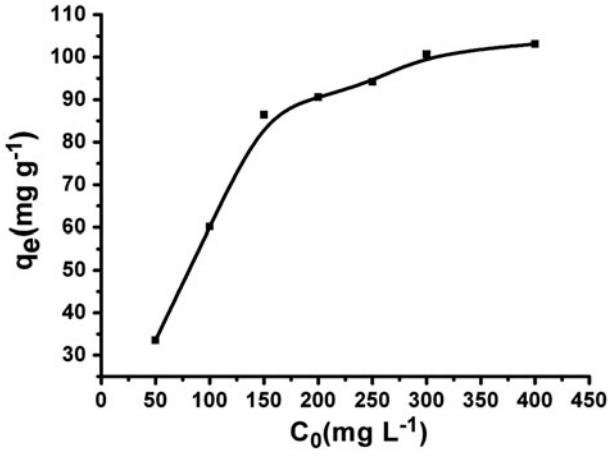

Fig. 6. Effect of the initial MB concentration.

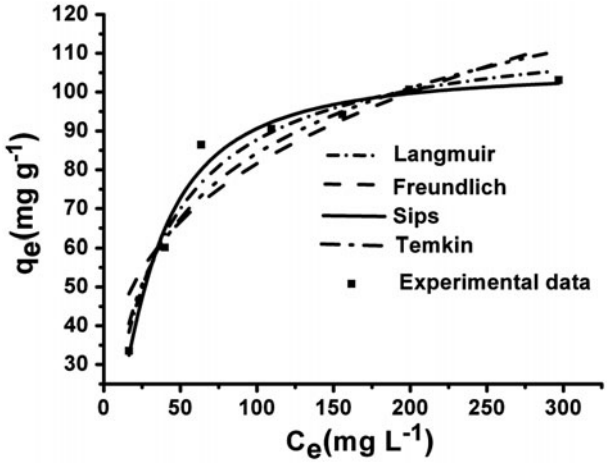

Fig. 7. Langmuir, Freundlich, Sips, and Temkin isotherms for adsorption of MB on EMC.

$$q_e = K_F C_e^{\frac{1}{n}} \quad (8)$$

Where C_e is the equilibrium methylene blue concentration (mg L^{-1}), q_e is the adsorption capacity at equilibrium (mg g^{-1}), K_F is the Freundlich adsorption constant (L mg^{-1}), and $1/n$ is the heterogeneity factor.

In order to resolve the problem of continuing increase in the adsorbed amount with a rising concentration as observed for Freundlich model, Sips isotherm model is proposed, differing only on the finite limit of adsorbed amount at sufficiently high concentration. It can be given as

$$q_e = \frac{q_m K_{eq} C_e^n}{1 + K_{eq} C_e^n} \quad (9)$$

where C_e is the equilibrium methylene blue concentration (mg L^{-1}), K_{eq} represents the equilibrium constant of the Sips equation (L mg^{-1}), and q_m is the maximum adsorption capacity (mg g^{-1}). The parameter n, stemming from the adsorbent or the dye or a combination of both, is regarded as the parameter characterizing the system's heterogeneity. If n is unit, the Sips isotherm equation turns into the Langmuir equation and it implies a homogeneous adsorption process.

The Temkin isotherm considers the interactions between adsorbents and dyes to be adsorbed and is based on the assumption that the free energy of adsorption is a function of the surface coverage [30]. The isotherm model is written as:

$$q_e = \frac{RT}{b_T} \ln(a_T C_e) \quad (10)$$

where a_T is the equilibrium binding constant corresponding to the maximum binding energy, b_T is the Temkin isotherm constant, T is the temperature (K), and R is the ideal gas constant (8.314 J mol^{-1} K^{-1}).

Fig. 7 shows the equilibrium adsorption of MB onto the EMC and the nonlinear fitting plot of four isotherm models. As is shown, the Sips isotherm correlated best ($R^2 = 0.9698$) with the experimental data from adsorption equilibrium of MB by EMC in the four models. Furthermore, the model parameters obtained by four models to the experimental data are given in Table 3. The equilibrium adsorption capacity

Table 3
Nonlinear fitting parameters of four isotherm equations

Langmuir				Freundlich		
q_m (mg g^{-1})	b (L mg^{-1})	R^2	R_L	$1/n$	k_F	R^2
117.5276	0.02946	0.9557	0.1016	0.2913	21.3372	0.8216
Sips				Temkin		
q_m (mg g^{-1})	K_{eq}	n	R^2	b_T	a_T	R^2
105.8077	0.0078	1.4432	0.9698	105.7718	0.3241	0.9066

($q_m = 105.8077\,mg\,g^{-1}$) obtained from Sips model is closer to the experimentally observed equilibrium capacity. It further demonstrated that the Sips adsorption isotherm is more suitable to explain the adsorption of MB onto EMC.

The Langmuir constant b can be used to determine the suitability of the adsorbent for the sorbate using the Hall separation factor (R_L) as follows [31]:

$$R_L = \frac{1}{1 + bC_m} \tag{11}$$

where C_m is the highest initial methylene blue concentration (mg L^{-1}), the value of R_L indicates the type of isotherm to be irreversible ($R_L = 0$), favorable ($0 < R_L < 1$), linear ($R_L = 1$) or unfavorable ($R_L > 1$) [32].

The value of R_L in the present investigation has been found to be 0.1016, indicating that the adsorption of MB onto EMC is favorable.

3.6. Effect of temperature and thermodynamic analysis

The adsorption process was studied while the reaction temperature was from 15 to 45℃. As shown in Fig. 8, there are apparent influences of temperature towards the adsorption capacity of MB. Within low temperature range ($T < 35$℃), the uptake capacity increased with increasing temperature. The maximum uptake capacity ($112.0580\,mg\,g^{-1}$) was obtained at 35℃. This could be attributed to increase in the mobility of MB, the enhancement in the deprotonation degree of active groups presented on the EMC surface and the acidity constant K_a of EDTA with increasing temperature. Meanwhile, higher temperature may facilitate the ionization effect of the EMC surface functional groups, resulting in the enhanced uptake capacity. However, the adsorption capacity decreased gradually when temperature exceeded 35℃. Obviously, some other factors would be responsible for the result. It seems that the major force (i.e. electrostatic interactions) involved in MB binding might be weakened by increasing temperature because electrostatic interactions are exothermic [22]. Furthermore, as the hydrolysis degree of the ester bond between EDTA molecules and hydroxyl/amino groups on the surface of EMC increased with increasing temperature, some EDTA molecules could be divorced from EMC. Therefore, the adsorption capacity of EMC for MB decreased rapidly at higher temperature.

3.7. FTIR analysis

The FTIR spectra play an important role in the analysis of these organic functional groups and the mechanism of MB ions adsorbed by the adsorbent [33,34]. Fig. 9 shows the FTIR spectra of chitosan, EMC before and after adsorbed MB. The peaks at 550 and 570 cm^{-1} were assigned to Fe–O bond vibration of Fe_3O_4. As shown in Fig. 9(a), the absorption band at around 3,440 cm^{-1} belonged to the stretching vibration of N–H group bonded with O–H group in chitosan. The peak at 1,593 cm^{-1} confirmed the N-H scissoring from the primary amine, due to the free amino groups in cross-linked chitosan. The bands at 1,420, 1,380, and 1,080 cm^{-1} were related to amide II, C–OH, and O–H groups, respectively. The increasing intensities at 1,598 and 1,403 cm^{-1} in the spectrum of EMC (seen in Fig. 9(b)) demonstrate that EMC had more C–OH and amine groups than chitosan. The result indicates that the EMC was cross-linked and

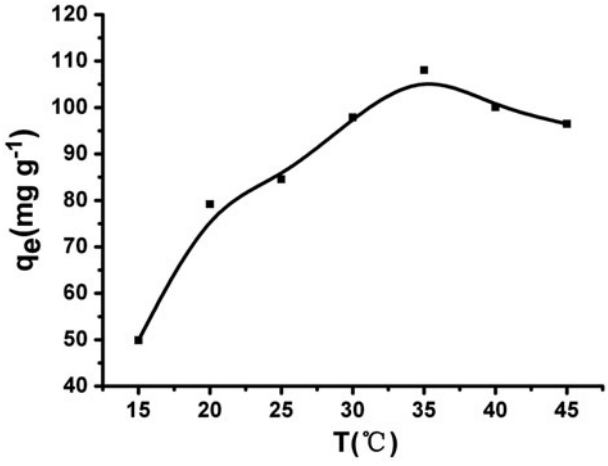

Fig. 8. Effect of temperature.

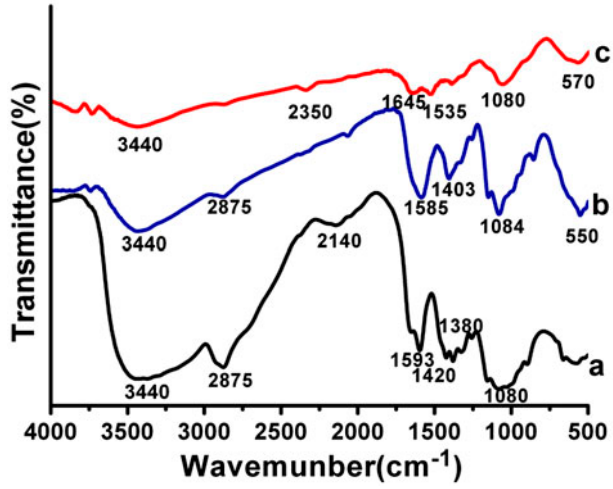

Fig. 9. FTIR spectra for chitosan (a), EMC before (b), and after (c) adsorbed MB.

Table 4
Desorption and regeneration results by different eluents

Eluents	Adsorption/desorption cycle	EMC regeneration efficiency (%)	MB recovery efficiency (%)
HCl (0.05 mol L^{-1})	1	94.20	95.37
	2	87.83	89.44
	3	82.82	80.72
HAc (0.05 mol L^{-1})	1	90.01	92.03
	2	80.56	85.24
	3	78.46	77.38
Absolute ethanol	1	87.57	88.27
	2	80.29	82.32
	3	74.03	73.56

modified with EDTAD successfully. The IR spectrum of EMC-adsorbed MB is given in Fig. 9(c). The adsorption intensity of broad strong peak at around 3,440 cm^{-1} decreased distinctly. One possible explanation is that –NH/–OH groups participated in the adsorption of MB. The peaks at 1,645, 1,535, and 1,080 cm^{-1} replaced the peaks at 1,585, 1,403, and 1,084 cm^{-1}, respectively. The decreasing adsorption intensity of the 1,645, 1,535, and 1,080 cm^{-1} compared with EMC indicates that the functional groups, such as carboxyl, amine, and hydroxyl groups presented on the surface of EMC, were responsible for the adsorption of MB.

3.8. Desorption and regeneration studies

Desorption and regeneration experiments were carried out in this study. The adsorption/desorption cycles of MB were repeated three times using HAc (0.05 M), HCl (0.05 M) solution, and absolute ethanol, the results obtained are given in Table 4. It could be found that the regeneration and recovery efficiency for EMC followed a decreasing order: HCl > HAc > absolute ethanol. As a typical strong acid, HCl solution could ionize more protons compared with HAc solution and absolute ethanol. The resulting H^+ ions would competitively occupy adsorption sites, thereby releasing MB ions. Consequently, the EMC could be used repeatedly with higher adsorption capacity and there were high desorption efficiency for MB by using HCl solution as the ideal elute.

4. Conclusions

EMC, as a potential reusable dye adsorbent, was prepared by chitosan coated by nano-Fe_3O_4 and EDTAD. The MB adsorption properties were investigated in our study.

The results showed that the maximum adsorption capacity (113.257 mg g^{-1} at pH 6.0, 300 mg L^{-1}) was obtained at 35˚C. The kinetic and equilibrium data were explained adequately by the pseudo-second-order kinetic model and the Langmuir isotherm model, respectively. Moreover, the results of potentiometric titration and FTIR indicate that the functional groups such as carboxyl, hydroxyl, and amine on EMC were responsible for MB adsorption. Meanwhile, the EMC could be recycled easily by an extra magnetic field and regenerated for reusing. Regeneration studies showed that the HCl (0.05 M) was the optimal eluent.

Acknowledgements

The authors would like to thank the financial supports of the Key Basic Research Program of Sichuan Provincial Education Commission, PR China (Grant No. 09ZA062) and the Innovation Research Program of the Science & Technology Department of Sichuan Province, PR China (Grant No. 091062630). Sincere thanks go to anonymous reviewers for helpful suggestions.

References

[1] H. Metivier-Pignon, C. Faur-Brasquet, P.L. Cloirec, Adsorption of dyes onto activated carbon cloths: approach of adsorption mechanisms and coupling of ACC with ultra filtration to treat coloured wastewaters, Sep. Purif. Technol. 31 (2003) 3–11.
[2] K. Ravi, B. Deebika, K. Balu, Decolourization of aqueous dye solutions by a novel adsorbent: application of statistical designs and surface plots for the optimization and regression analysis, J. Hazard. Mater. 122 (2005) 75–83.
[3] I.A.W. Tan, A.L. Ahmad, B.H. Hameed, Adsorption of basic dye on high-surface area activated carbon prepared from coconut husk: Equilibrium, kinetic and thermodynamic studies, J. Hazard. Mater. 154 (2008) 337–346.
[4] I.A.W. Tan, A.L. Ahmad, B.H. Hameed, Adsorption of basic dye using activated carbon prepared from oil palm shell: batch and fixed bed studies, Desalination 225 (2008) 13–28.
[5] A.K. Jain, V.K. Gupta, A. Bhatnagar, Suhas, Utilization of industrial waste products as adsorbents for the removal of dyes, J. Hazard. Mater. 101 (2003) 31–42.
[6] Y. Tian, C.Y. Ji, M.J. Zhao, M. Xu, Y.S. Zhang, R.G. Wang, Preparation and characterization of baker's yeast modified by nano-Fe_3O_4: Application of biosorption of methyl violet in aqueous solution, Chem. Eng. J. 165 (2010) 474–481.
[7] Z.J. Hu, N.X. Wang, J. Tan, J.Q. Chen, W.Y. Zhong, Kinetic and equilibrium of cefradine adsorption onto peanut husk, Desalin. Water Treat. 37 (2012) 160–168.
[8] T.Y. Guo, Y.Q. Xia, G.J. Hao, B.H. Zhang, G.Q. Fu, Z. Yuan, B.L. He, J.F. Kennedy, Chemically modified chitosan beads as matrices for adsorptive separation of proteins by molecularly imprinted polymer, Carbohydr. Polym. 62 (2005) 214–221.
[9] M. Rutnakornpituk, P. Ngamdee, P. Phinyocheep, Preparation and properties of polydimethylsiloxane-modified chitosan, Carbohydr. Polym. 63 (2006) 229–237.

[10] A. Ramesh, H. Hasegawa, W. Sugimoto, T. Maki, K. Ueda, Adsorption of gold (III), platinum (IV) and palladium (II) onto glycine modified crosslinked chitosan resin, Bioresour. Technol. 99 (2008) 3801–3809.
[11] L. Wang, R. Xing, S. Liu, Y.K. Qin, K.C. Li, H.H. Yu, R.F. Li, P.C. Li, Studies on adsorption behavior of Pb(II) onto a thiourea-modified chitosan resin with Pb(II) as template, Carbohydr. Polym. 81 (2010) 305–310.
[12] J.S. Wang, R.T. Peng, J.H. Yang, Y.C. Liu, X.J. Hu, Preparation of ethylenediamine-modified magnetic chitosan complex for adsorption of uranyl ions, Carbohydr. Polym. 84 (2011) 1169–1175.
[13] M. Monier, D.M. Ayad, Y. Wei, A.A. Sarhan, Adsorption of Cu(II), Co(II), and Ni(II) ions by modified magnetic chitosan chelating resin, J. Hazard. Mater. 77 (2010) 962–970.
[14] L.M. Zhou, J.P. Xu, X.Z. Liang, Z.R. Liu, Adsorption of platinum(IV) and palladium (II) from aqueous solution by magnetic cross-linking chitosan nanoparticles modified with ethylenediamine, J. Hazard. Mater. 182 (2010) 518–524.
[15] D. Hritcu, D. Humelnicu, G. Dodi, M.I. Popa, Magnetic chitosan composite particles: Evaluation of thorium and uranyl ion adsorption from aqueous solutions, Carbohydr. Polym. 87 (2012) 1185–1191.
[16] C.S. Shen, Y. Shen, Y.Z. Wen, H.Y. Wang, W.P. Liu, Fast and highly efficient removal of dyes under alkaline conditions using magnetic chitosan-Fe (III) hydrogel, Water Res. 45 (2011) 5200–5210.
[17] X.X. Wang, S. Huang, Z. Shan, Preparation of Fe_3O_4@Au nano-composites by self-assembly technique for immobilization of glucose oxidase, Chin. Sci. Bull. 54 (2009) 1176–1181.
[18] Osvaldo Karnitz Júnior Leandro Vinícius Alves Gurgel, Rossimiriam Pereira de Freitas, Laurent Frédéric Gil, Adsorption of Cu(II), Cd(II), and Pb(II) from aqueous single metal solutions by mercerized cellulose and mercerized sugarcane bagasse chemically modified with EDTA dianhydride (EDTAD), Carbohydr. Polym. 77 (2009) 643–650.
[19] S.Q. Memon, N. Memon, S.W. Shah, M.Y. Khuhawar, M.I. Bhanger, Sawdust-a green and economical sorbent for the removal of cadmium(II) ions, J. Hazard. Mater. 139 (2007) 116–121.
[20] P. Lodeiro, A. Fuentes, R. Herrero, D.E. Sastre, M.E. Vicente, Cr(III) binding by surface polymers in natural biomass: the role of carboxylic groups, Environ. Chem. 5 (2008) 355–365.
[21] A. Barkleit, H. Moll, G. Bernhard, Interaction of uranium(VI) with lipopolysaccharide, J. Chem. Soc. 21 (2008) 2879–2886.
[22] Y.S. Zhang, W.G. Liu, M. Xu, F. Zheng, M.J. Zhao, Study of the mechanisms of Cu^{2+} biosorption by ethanol/caustic-pretreated baker's yeast biomass, J. Hazard. Mater. 178 (2010) 1085–1093.
[23] G.Y. Li, Y.R. Jiang, K.L. Huang, Ding, Jie Chen, Preparation and properties of magnetic Fe_3O_4-chitosan nanoparticles, J. Alloy. Compd. 466 (2008) 45–456.
[24] H.V. Tran, L.D. Tran, T.N. Nguyen, Preparation of chitosan/magnetite composite beads and their application for removal of Pb(II) and Ni(II) from aqueous solution, Mater. Sci. Eng. C30 (2010) 304–310.
[25] Y.S. Zhang, W.G. Liu, L. Zhang, M. Wang, M.J. Zhao, Application of bifunctional *Saccharomyces cerevisiae* to remove lead (II) and cadmium(II) in aqueous solution, Appl. Surf. Sci. 257 (2011) 9809–9816.
[26] M. Yurdakoc, Y. Scki, S.K. Yuedakoc, Kinetic and thermodynamic studies of boron removal by Siral 5, Siral 40, and Siral 80, J. Colloid Interface Sci. 286 (2005) 440–446.
[27] F.C. Wu, R.L. Tseng, R.S. Juang, Kinetic modeling of liquid-phase adsorption of reactive dyes and metal ions on chitosan, Water Res. 35 (2001) 613–618.
[28] C. Ferdaõg, N. Olaka, A. Atarb, Olgunb, Biosorption of acidic dyes from aqueous solution by *Paenibacillus macerans*: Kinetic, thermodynamic and equilibrium studies, Chem. Eng. J. 150 (2009) 122–130.
[29] H. Parab, S. Joshi, N. Shenoy, R. Verma, A. Lali, M. Sudersanan, Uranium removal from aqueous solution by coir pith: Equilibrium and kinetic studies, Bioresour. Technol. 96 (2005) 1241–1248.
[30] M. Monier, D.M. Ayad, Y. Wei, A.A. Sarhan, Adsorption of Cu(II), Co(II), and Ni(II) ions by modified magnetic chitosan chelating resin, J. Hazard. Mater. 177 (2010) 962–970.
[31] R. Nadeem, M.A. Hanif, F. Shaheen, S. Perveen, M.N. Zafar, T. Iqbal, Physical and chemical modification of distillery sludge for Pb(II) biosorption, J. Hazard. Mater. 150 (2008) 335–342.
[32] S. Dahiya, R.M. Tripathi, A.G. Hegde, Biosorption of heavy metals and radionuclide from aqueous solutions by pre-treated arca shell biomass, J. Hazard. Mater. 150 (2008) 376–386.
[33] K. Chauhan, G.S. Chauhan, J.H. Ahn, Synthesis and characterization of novel guar gum hydrogels and their use as Cu^{2+} sorbents, Bioresour. Technol. 100 (2009) 3599–3603.
[34] M. Bansala, U. Garg, D. Singh, V.K. Garg, Removal of Cr(VI) from aqueous solutions using pre-consumer processing agricultural waste: A case study of rice husk, J. Hazard. Mater. 162 (2009) 312–320.